# Stress and strain behavior investigation on a scale model geotextile tube for Saemangeum dike project

Hyeong-Joo Kim[1a], Kwang-Hyung Lee[*2], Sung-Kyeong Jo[2b] and Jay C. Jamin[2c]

[1]*Department of Civil Engineering, Kunsan National University, Gunsan 573-701, Republic of Korea*
[2]*Department of Civil and Environmental Engineering, Kunsan National University, Gunsan 573-701, Republic of Korea*

**Abstract.**   Geotextile tubes are basically a huge sack filled with sand or dredged soil. Geotextile tubes are made of permeable woven or non-woven synthetic fibers (i.e., polyester or PET and polypropylene or PP). The geotextile tubes' performances in strength, dewatering, retaining solid particles and stacked stability have been studied extensively in the past. However, only little research has been done in the observation of the deformation behavior of geotextile tubes. In this paper, a large-scale apparatus for geotextile tube experiment is introduced. The apparatus is equipped with a slurry mixing station, pumping and delivery station, an observation station and a data station. For this study the large-scale apparatus was utilized in the studies regarding the stresses on the geotextile and the deformation behavior of the geotextile tube. Model tests were conducted using a custom-made woven geotextile tubes. Load cells placed at the inner belly of the geotextile tube to monitor the total soil pressure. Strain gauges were also placed on the outer skin of the tube to measure the geotextile strain. The pressure and strain sensors are attached to a data logger that sends the collected data to a desktop computer. The experiment results showed that the maximum geotextile strain occurs at the sides of the tube and the soil pressure distribution varies at each geotextile tube section.

**Keywords:**   geotextile tube; stress; strain; scale model test

## 1. Introduction

Geotextile tubes are widely used in South Korea since the late 1990s up to the present. At present, geotextile tubes are applied as containment dikes for the reclamation project at Saemangeum (Fig. 1(a)). The Saemangeum comprehensive development project begun in 1991 where a 33.9 km sea dike was constructed in a span of 15 years. A land area of about 283 km$^2$ is projected to be reclaimed at Saemangeum dedicated for the development of facilities for businesses, industry, agriculture and tourism in the near future. The development plan for the Saemangeum project is shown in Fig. 1(b).

Presently, the annual consumption of cement and concrete has significantly increased in South

---

∗Corresponding author, Ph.D. candidate, E-mail: kwanghyung@naver.com
[a] Professor, E-mail: kimhj@kunsan.ac.kr
[b] Graduate student, E-mail: 1310108@kunsan.ac.kr
[c] Graduate student, E-mail: jaminjc@kunsan.ac.kr

Korea. There is a decreasing supply of cement and construction aggregates such as rock, gravel and sand whose quantities are now limited due to environmental restrictions in the quarry site. Construction expenses have also increased due to additional delivery costs from source to site and construction time is longer due to may process and equipment involved. Geotextile tube technology could be a viable alternative to the conventional ruble mound structures in cases where temporary protection is required or rock is not obtainable and difficult to transport to the site.

Geotextile tubes are made from strong and flexible textile materials that are capable of retaining fine-grained materials though permeable enough to allow the excess water from the hydraulically filled slurry to dissipate. Geotextile tubes have been effectively and increasingly applied mainly in coastal and hydraulic engineering fields as an alternative for the conventional pre-cast concrete-made and natural rock-made structures. In recent years geotextile tubes were used as groynes and breakwaters to protect or mitigate shoreline/coastline erosions (Cantré 2002, Gibeaut *et al*. 2003, Alvarez *et al*. 2007, Pilarczyk 2008, Parab *et al*. 2011), as containment dikes for land reclamation and man-made islands (Fowler et al., 2002a; 2002b), and as revetments acting as mass-gravity barrier-type structures and protection dikes to prevent damage tovaluable structures caused by natural calamities (Restall *et al*. 2002, Lawson, 2008).

Geotextile tubes have been of interest in various studies due to its wide applications in civil engineering. Evaluation results on the permeability and retention characteristics of geotextile tubes can be found in the studies of Moo-Young *et al*. (2002), Koerner and Koerner (2006) and Weggel *et al*. (2011). Model tests and large-scale experiments on geotextile tubes can be found in the literature (Recio and Oumeraci, 2009, Kriel 2012, Kim *et al*. 2013b, 2014a, b). Numerical (Kim *et al*. 2013a, 2014b) and analytical methods (Plaut and Klusman 1999) were also conducted to study the stability of stacked geotextile tubes. In general the studies available in the literature focuses on the investigation of the hydraulic stability of stacked geotextile tubes and the geotextile performance in strength, durability and permeability. However, very little is presently understood about the consolidation behavior of the fill materials and the stress and strain behavior of the confining geotextile. Brink *et al*. (2013) has proposed a consolidation modelling method for geotextile tubes filled with fine-grained materials. Cantré and Saathoff (2011) has numerically formulated a design method for tubes considering the geotextile strain.



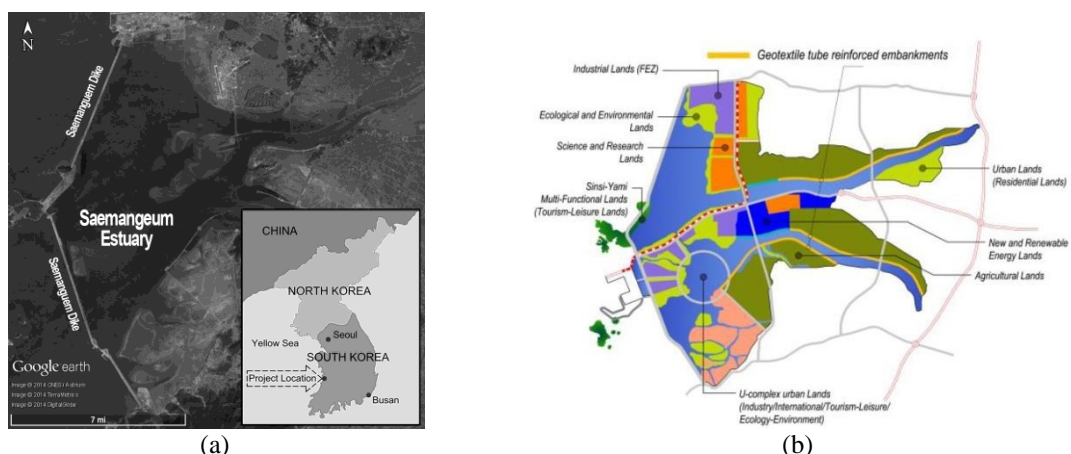(a)                                              (b)

Fig. 1 (a) Project location (Image© Google, Image © 2014 CNES/Astrium, Image © 2014 TerraMetrics, Image © 2014 DigitalGlobe); (b) site development plan

It is particularly difficult to determine analytically the applied stresses on the skin and on the fill material due to its erratic nature of geotextile tubes during the filling and dewatering stages. Conventionally, assumptions such as the generation of uniform circumferential tensile stress (Liu and Silvester 1977, Leshchinsky *et al.* 1996, Plaut and Suherman 1998) are established in order to simplify the analysis. The objective of the present study is to investigate experimentally the characteristics of the fill material, the shape deformation behavior of the tube, the geotextile strain and the variation of stresses in the internal soil mass. The experiment results can then be used for numerical validations in the future studies. Also, in this paper, a large-scale apparatus for geotextile tube experiments is introduced. The apparatus is equipped with a mixing station, pumping and delivery station, an observation station and a data station. This apparatus is specifically designed for large-scale experimental studies on the geotextile tube deformation behavior under dry and submerged conditions.

Results from the geotextile tube test using a large-scale apparatus are presented in this paper. The study focused on the observation of the redistribution of the fill material in the tube and its effect to the shape deformation of the geotextile tube. In addition, a T-type inlet system was used during the experiment. Instead of conventionally feeding directly the slurry into the geotextile tube (where the pumping pressure is directly perpendicular to the circumferential tensile force of the geotextile), the T-type inlet system enables the slurry to be deflected in two opposite directions along the geotextile tube length, hence, theoretically reducing the intensity of the pumping pressure acting on the circumferential length of the geotextile tube.


## 2. Laboratory setup and procedure

### 2.1 Large-scale apparatus

The large-scale apparatus shown in Fig. 2 is equipped with a mixing station, pumping and delivery station, and an observation station. The mixing station comprises of a ① mixing tank and ② water supply tank. Soil (dredged soil or sand) and water are combined in the mixing tank for the slurry preparation. An electric agitator composed of a shaft rod attached to an electric motor at one end and an impeller at the other end is installed above the mixing tank. The electric agitator blends the soil and water mixture until a slurry material is produced. In the pumping and delivery station a ③ hydraulic pump is used to draw the slurry from the mixing tank via the ④ two-way slurry delivery pipe system during the filling process. There are two filling options for the slurry into the geotextile tube, through direct hydraulic pumping or via the ⑤ gravity tank. For the hydraulic filling, the slurry is hydraulically pumped into the geotextile tube. Alternatively, geotextile filling by gravity initially requires pumping the slurry from the mixing tank to the gravity tank. An electric agitator is also installed on top of the gravity tank to continually agitate the slurry mixture. To fill the geotextile tube, a gate valve at the bottom of the tank is opened and the slurry is filled through gravitation. In the case of gravity filling, the pumping pressure will be based on the hydraulic head of the slurry in the gravity tank. The hydraulic head will be equal to the difference between the elevation of the filling port and the elevation of the slurry surface. For the present study, the geotextile tubes were filled hydraulically. The experimental observations for the geotextile tube models are made in the observation station or the ⑥ test tank. The steel tank floor has dimensions of 3 m x 5 m and can be filled with water at a maximum height of 1.5 meters

to simulate geotextile tube models under submerged conditions. In both submerged and non-submerged geotextile tube test cases, water from the test tank can be recycled and reused for the next experiment by pumping out the water back to the water supply tank using submersible water pumps.

### 2.2 Dredged fill and geotextile properties

The fill material used in the present study was obtained from a local dredging area at Saemangeum, located at the west coast of South Korea. The dredged soil fill used for the geotextile tube test is classified as a non-plastic silty-sand (SM) in accordance with the Unified Soil Classification System. Physical properties of the dredged soil are shown in Table 1 and the grain size distribution curve is shown in Fig. 3.
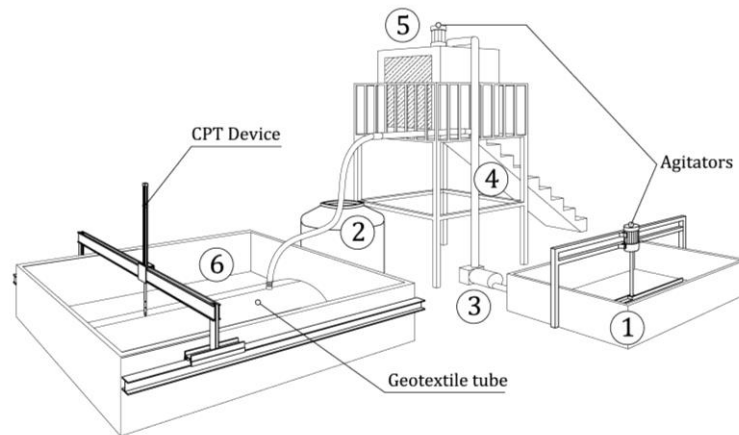
Fig. 2 Experiment setup schematic

Table 1 Physical properties of the dredged soil fill

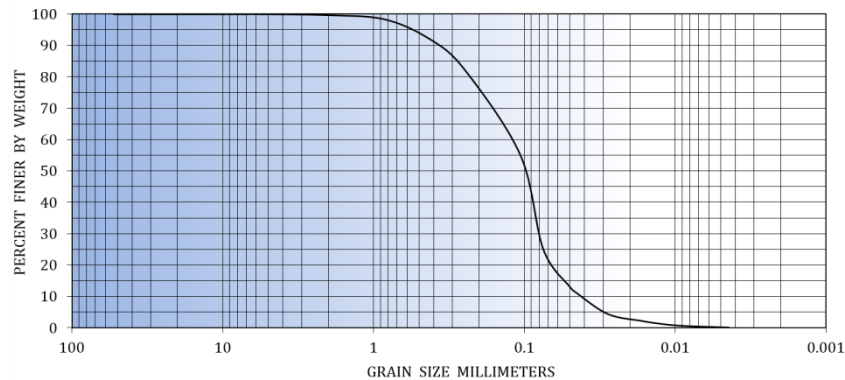| Item | Quantity |
| --- | --- |
| Natural water content, wn (%) | 15.9 |
| Specific gravity of soil solids, Gs | 2.69 |
| Plasticity Index, PI (%) | N.P.* |
| Percent passing #200 sieve | 25 |
| Soil classification (USCS) | SM** |

*Non-plastic; **silty-sand

Fig. 3 Grain size distribution curve

Table 2 Woven Geotextile Properties

| Description | Unit | Quality/Quantity |
| --- | --- | --- |
| Material Type | - | PP (Polypropylene) |
| Thickness | mm | 2.0 |
| Elongation | % | 13 ~ 14 |
| Tensile Strength | | |
| *Longitudinal* | kN/m | 195 |
| *Transverse* | kN/m | 180 |

The geotextile tube used in the present study is made of a woven P.P. (polypropylene) geotextile material. The geotextile tube is 4.0 m long and has a theoretical diameter of 1.0 m. The physical properties of the geotextile tube are shown in Table 2. The geotextile tensile strength-strain relationship obtained from a laboratory test of the P.P. material is shown in Fig. 4. Initially the polypropylene geotextile is strained up to 15% with minimal force. This can be attributed to the realignment of loose geotextile fibers at start of the application of the tensile force.

The geotextile tube used in this study was custom-built. First, a sheet of P.P. geotextile tube was measured and cut according to the desired specifications as shown in Fig. 5(a). In the case of the present study, the geotextile sheet obtained was not sufficient enough to form the desired geotextile tubedimension; hence, two separate sheets of geotextile were attached first. The seams connecting the two sheets of geotextile joined using 6 rows of stiches. Sequentially, the ends of the joined geotextile sheet in the longitudinal direction are attached and sewn similarly using 6 rows of stiches. The stitching of the geotextile tube seams is shown in Fig. 5(b). The finished tube is shown is Fig. 5(c). The height and width measurements for the geotextile tube are shown in Fig. 5(d).
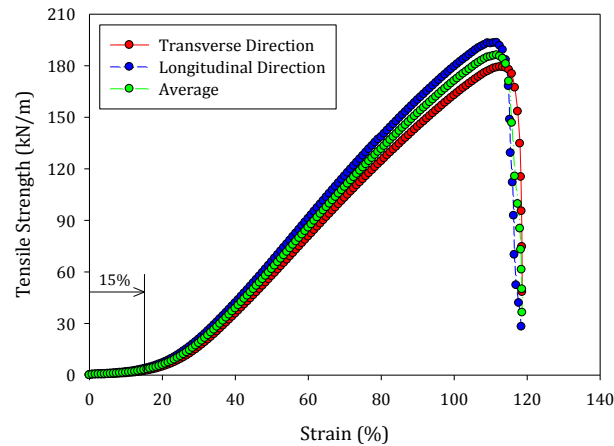
Fig. 4 P.P. geotextile tensile strength-strain relationship
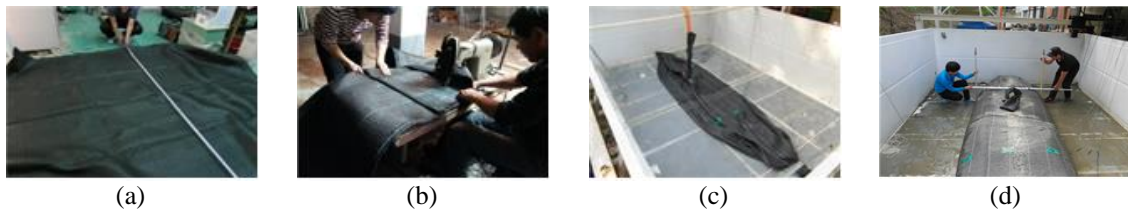


| (a) | (b) | (c) | (d) |

Fig. 5 Geotextile tube fabrication. (a) Measuring and cutting, (b) sewing the textile seams, (c) actual placement of the tube in the test tank and (d) height and width measurements during filling/dewatering process

## 2.3 Placement of measuring devices and experiment procedures

### 2.3.1 Strain gauge and soil pressure sensor placement

Strain gauges are also placed on the outer skin of the geotextile. Details for the location and placement of the pressure and strain sensors are shown in Fig. 6. The strain gauge and pressure cell readings were collected by the data logger and interpreted by a desktop computer in the data station. The strain gauge is attached to the geotextile skin in the same manner shown in Fig. 6(a) along the transverse direction of the tube to measure the tube's circumferential strain. The surface of the geotextile area where the strain gauge will be attached should be cleaned. Then a sufficient amount of chloroprene (CR) adhesive (occupies at least about an area of 20 mm x 50 mm) is spread on the surface of the geotextile skin. The strain gauge is then placed on top of the applied CR adhesive. After the strain gauge is secured, an N-1 coating is coated on top of the strain gauge to cover the device. Lastly, the attachment is covered with a VM tape for waterproofing. In this study, four strain gauges were attached to the tube in the same manner as shown in Fig. 6(b). The section in the geotextile tube where the strain gauges are placed is shown in Fig. 7(a).
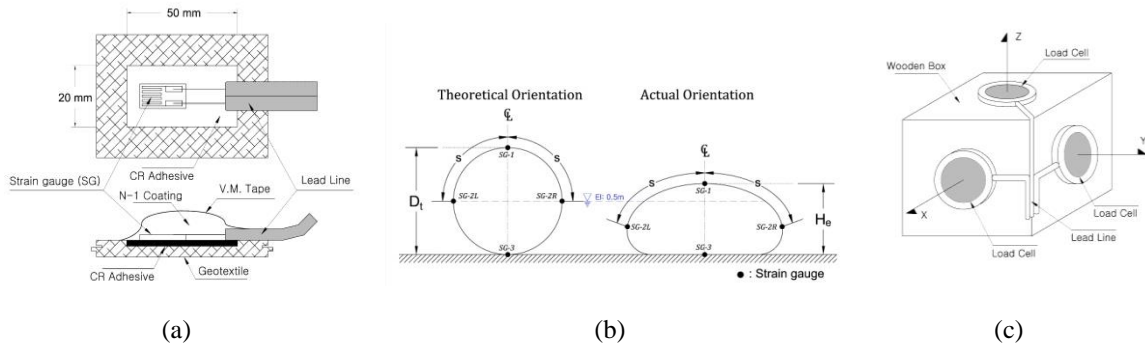
Fig. 6 (a) Strain gauge installation details, (b) strain gauge positioning on the geotextile tube and (c) load cell details
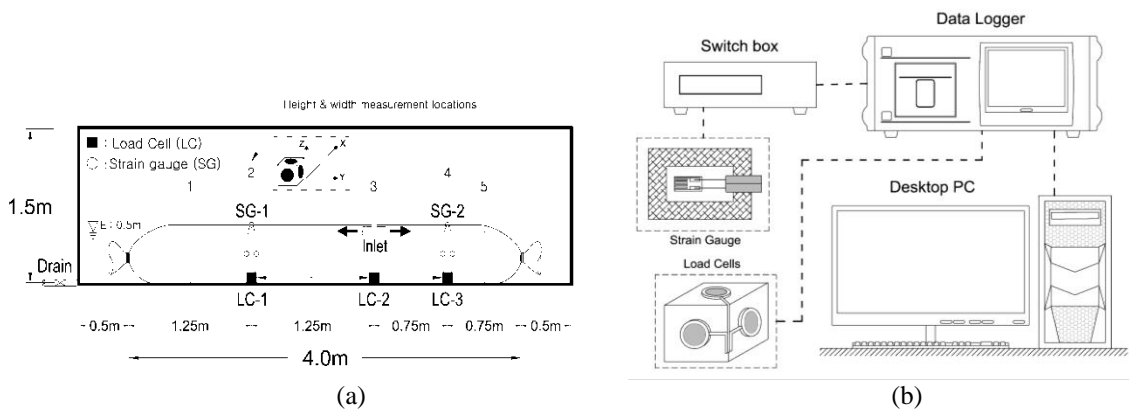


Fig. 7 (a) Strain Gauge and Load Cell placement and (b) Data station

Load cells or soil pressure meters (Model: FSP-2) are placed inside the geotextile tubes to measure the total soil pressure in the x, y and z directions. To do this, the cells are attached on a wooden box as shown in Fig. 6(c). Three of these modified pressure cell apparatus are placed inside the tube to measure the soli pressure at the bottom. The pressure cell placement in the tube is shown in Fig. 7(a). The maximum load capacity for each soil pressure meter is 196 kPa (as per manufacturer's specification).

### 2.3.2 Test procedures

In preparation for the slurry fill the dredged soil and water are combined in the mixing tank. 3:1 water to soil ratio slurry mixture (300% water content) is used for both geotextile tube experiments. The mixture was continually stirred by the electric agitator to achieve an even mixture and retain the desired slurry consistency.  Concurrent with the slurry preparation, the geotextile tube is placed into position inside the test tank (Fig. 5◎ ). The geotextile tube is filled hydraulically. The

slurry is pumped into the geotextile tube through the improvised T-type inlet system during the filling phase. The tubes are filled, dewatered and refilled again until the dewatered height of the tube following the last filling phase is approximately equal to 40 ~ 50% the theoretical diameter of the geotextile tube. The pumping pressure during filling was maintained at 30kN/m2. Measurements of the tube height and width at each section are taken after filling (filled height and width) and before refilling (dewatered height and width) of slurry (Fig. 5(d)). The strain and pressure data are collected via a data logger and monitored through a desktop PC (Fig. 7(b)). After the filling and dewatering tests, soil samples were gathered from the topmost and bottom part of the tube. The water content and percent passing #200 sieve of these samples were determined to evaluate the variation of fill material characteristics in the tube.

## 3. Results and discussions

### 3.1 Fill material characteristics after the test

The physical properties of the fill material were determined after the filling and dewatering observations of the geotextile tube. The distribution of fine-grained soil in the tube is shown in Fig. 8a. On the upper layer of the soil deposit, most fines are heavily deposited further away from the inlet of the tube (location ③, please refer to Fig. 7(a)). The same is true with the soil deposits at the bottom layer. Fig. 8b shows the variation in the amount of water content of the soil fill. It is shown here that the amount of moisture content in the upper layer is substantially lower compared to that in the lower layer.
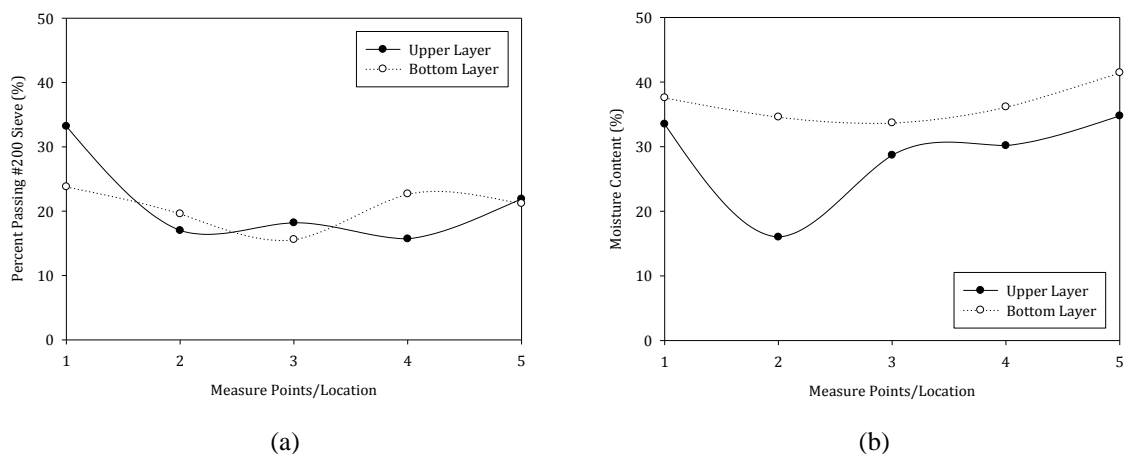


(a)                                             (b)

Fig. 8 Fill properties after the stabilization stage; (a) Percent passing #200 sieve and (b) water content

## 3.2 Geotextile tube shape

The recorded height and width of the tube at locations ② and ④ during the filling and dewatering process of the tube are shown in Figs. 9(a) and 9(b), respectively. It can be observed that as the tube height increases the width of the geotextile tube decreases during filling. Conversely, the tube height decreases and the tube width increases during the dewatering process. Fig. 10(a) illustrates the shape of the tube at locations ② and ④ after each filling stage. Both section measurements were taken at the same time. Evidently the tube height in both sections varies after each filling stage. The variation in the tube height and width can be attributed to the amount of fill material deposits in the area. Obviously, the section near the inlet (location ④) attains more soil deposits compared to the sections away from the inlet (location ②). However, in the stabilization stage, the magnitude of the tube height and width changes. During the stabilization stage significant decrease in the tube height is observed at location ④. This can be attributed to the amount fine soil and its moisture content in that area. As shown in Fig. 7, location ④ has a large amount of fine-grained soil deposits with high moisture content. Hence, as the water is expelled during the dewatering period for two days, the fine material occupies the space of the expelled water, thus, reducing the volume in that area. In location②, however, there is not much change in the tube height after two days stabilization. This is because coarse-grained particles are mostly present in that area. Hence during the dewatering process, only a little amount of water is dissipating from this area initiating a minute change in the volume in that location. The amount of the tube height and width after the filling process are summarized in Table 3.



(a)                                                                          (b)
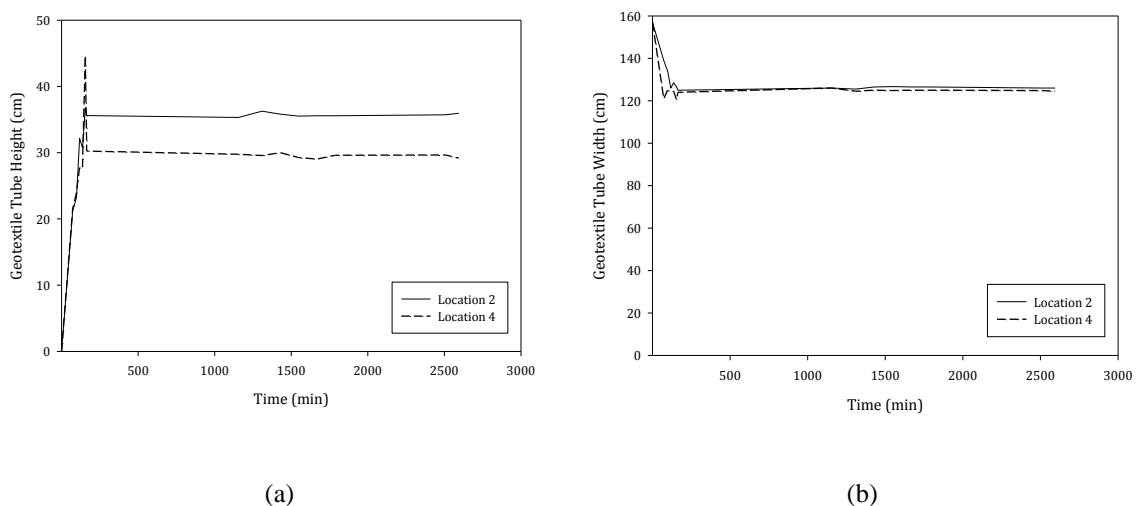
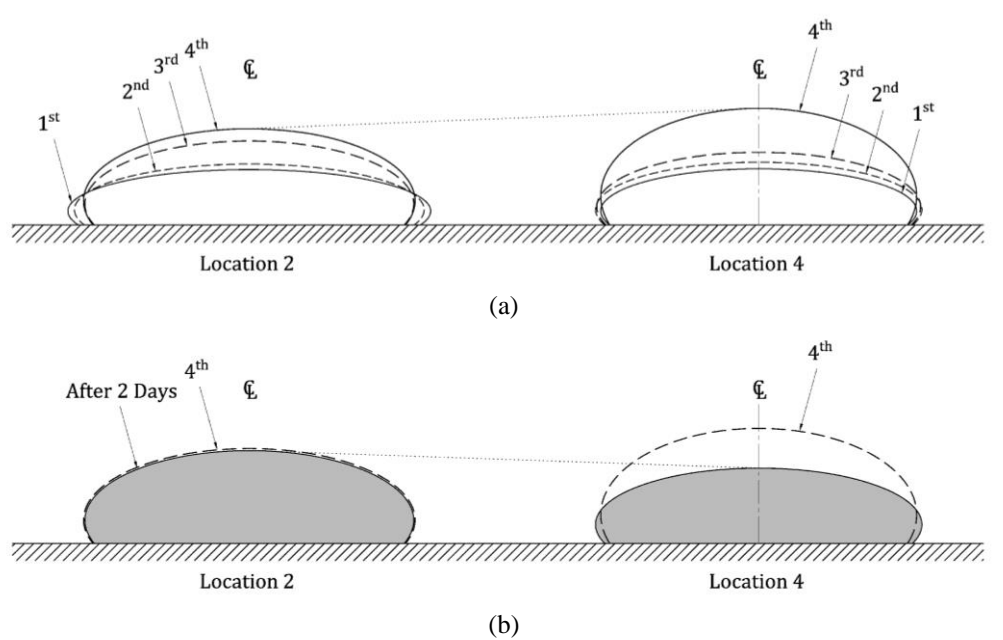Fig. 9 Variation in the geotextile tube's (a) height and (b) width

Fig. 10 Variation in the geotextile tube shape at Locations 2 & 4 during (a) filling stages and (b) stabilized stage

Table 3 Summary of the variation in the geotextile tube's shape properties

| Description | Property | Filling Stage | | | | Stabilized Stage |
|---|---|---|---|---|---|---|
| | | 1st | 2nd | 3rd | 4th | (after 2 days) |
| Location 2 | Height (mm) | 212 | 233 | 321 | 368 | 360 |
| | Width (mm) | 1390 | 1340 | 1260 | 1265 | 1260 |
| Location 4 | Height (mm) | 215 | 240 | 278 | 446 | 292 |
| | Width (mm) | 1210 | 1250 | 1240 | 1205 | 1245 |

### 3.3 Geotextile strain

Theoretically, it is assumed in the analysis that the geotextile strain only appears along the free perimeter $L_f$ of the tube where only elastic deformation occurs and the strains are considered to be constant (Cantré and Saathoff 2011). The free perimeter is the part of the geotextile tube's surface with no contact to the ground, that is

$$L_f = L_t - B \tag{1}$$

where $L_t$ is the total perimeter of the tube and $B$ is the contact length of the tube to the ground.

Therefore considering strain, the new total perimeter of the geotextile tube becomes

$$L_{tn} = L_{tp} + (L_t - B)\varepsilon_i \qquad (2)$$

where $L_{tn}$ is the new total perimeter, $L_{tp}$ is the previous total perimeter and $\varepsilon_i$ is the geotextile strain along the free perimeter.

During the experiment, the strain gauges were oriented along the transverse direction of the geotextile tube to monitor the development of circumferential strain. The data for the geotextile strain at SG-1 (please refer to Fig. 7(a)) is shown in Fig. 11(a). The readings indicates an increase in geotextile strain during the filling process and decreases during the dewatering process. Presumably, minimal geotextile strain occurs at the bottom due to the confining effect between the soil fill and foundation. At the beginning of the test, this assumption is proven accurate as represented by a dash-dot line in Fig. 11a. However, after 1000 min the magnitude of the strain at the bottom was reduced until it became less than that of the topmost strain of the geotextile tube. This might be due to some external factors such as water leakage unto the strain gauge device altering its performance after the 1000 min mark. Nevertheless, the reading for both the side and top strains shows a similar trend as time progresses. The same behavior is observed for the geotextile strain at SG-2 (Fig. 11(b)). Apparently the maximum strain occurs at the sides of the tube, followed by the strain at the top most portion. At the end of the experiment, the geotextile strain at the sides of the geotextile tube was found to be roughly 6.5 times that of the topmost geotextile strain.

The existing calculation methods available in the literature assumed that the circumferential tensile force of the geotextile container is constant (Liu and Silvester 1977, Leshchinsky *et al*. 1996, Plaut and Suherman 1998). This assumption was made in order to easily solve the plane strain membrane theory problem. For the present study, the reading for the topmost geotextile strain gauge is significantly low for both geotextile containers and the strain gauge data results shows a variation of strain deformation along its circumference. This suggests that in reality the circumferential tensile force that causes these deformations are non-uniform along the containers circumferential length. It should be noted that the fill material for the geotextile container considered in the theoretical analysis is fluid. Hence, in the case of the present study, the solidified soil fill may have an influence to the strain variation readings on geotextile tube's circumference.

### 3.4 Stress variations in the internal soil mass

As mention in section 2.3.1, three customized load cell devices were placed in the bottom part of the geotextile tube's interior. The contrivance consist of three pressure sensors oriented at directions x, y and z (i.e., x – along the width/transverse section of the tube; y – along the length/longitudinal section of the tube; z – vertical axis). The total pressure readings during the first 300mins of filling and dewatering process of the geotextile tube are shown in Fig. 12. Interestingly, the results for total pressure along the y-axis is higher than the total pressure on both x and z-axes. Also, the soil pressures along the x-axis are notably higher compared to the soil pressure along the z-axis. This phenomenon might be caused by the confinement effect of the soil sediments inside the geotextile tubes. The side strains, as mentioned in section 3.3, have the largest magnitude. This could suggest that the stresses at the sides of the geotextile tube have a higher magnitude. Hence, the soil fill are most likely pushed sideways rather than downwards due to the additional stress generated by the geotextile skin.

The fill material is assumed to be bounded by a frictionless geotextile membrane. The soil elements at any depth in the geotextile tube are subjected to vertical effective pressure, $\sigma'_v$, and horizontal effective pressure, $\sigma'_h$. The ratio between the effective vertical and horizontal pressures can be defined a non-dimensional $K$,

$$K = \frac{\sigma'_h}{\sigma'_v} \tag{3}$$

The variation in the coefficient of active lateral pressures ($K_{ax}$) at LC1-1 and LC-3 (please refer to Fig. 7(a) for the sensor orientation) are shown in Fig. 12. During the filling process, it can be seen that the coefficient of active lateral pressure varies in an increasing manner as time progresses. After the final filling process the coefficient of active pressure in both LC-1 and LC-3 normalizes as illustrated by the fitted points in Fig. 13. The coefficient of active lateral pressure near the inlet of the geotextile tube (LC-3) shows a greater magnitude compared to the section distant from the inlet (LC-1). It should be noted that the calculated coefficient of lateral pressure based on the measured data presented in this paper are unusually excessive. Generally, thecoefficient of active earth pressure for normally consolidated soils is less than 1 (Das 2010). However, for the case of the present study, the condition of the fill material is varied throughout the experiment (e.g., high moisture content soil or slurry form during filling, saturated fill during dewatering). Factors such as the transformation of the tubes cross-section and the variation of the moisture content may have possibly influenced this phenomenon. Another possible reason for this can be attributed to the compaction and confinement effect of the geotextile tube due to the dewatering process. During the dewatering stage, the tube height decreases and the tube width increases. This increases the density of the confined fill material and the tensile reaction of the tube. The compaction effect on top of the geotextile tube decreases as the tube height reduces. On the other hand, the confinement effect at the sides of the geotextile tube increases as the tensile reaction intensifies. As a result, the vertical pressure was decreased and the lateral pressures were increased, consequently increasing the coefficient of active earth pressure. This means that the contained fill material might fail and internally rearrange the soil particlesdue to the dewatering process. Therefore, in order to achieve external stability, the geotextile strength must be greater than that of the applied soil pressure.
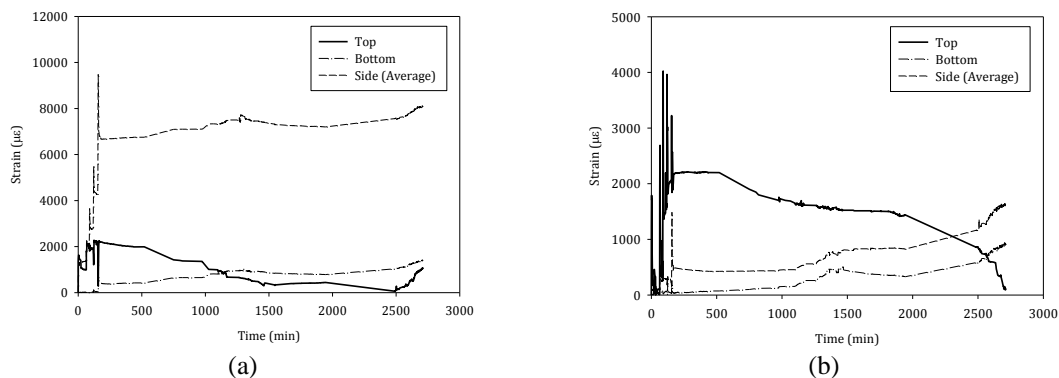


Fig. 11 Geotextile strain at (a) SG-1 and (b) SG-2
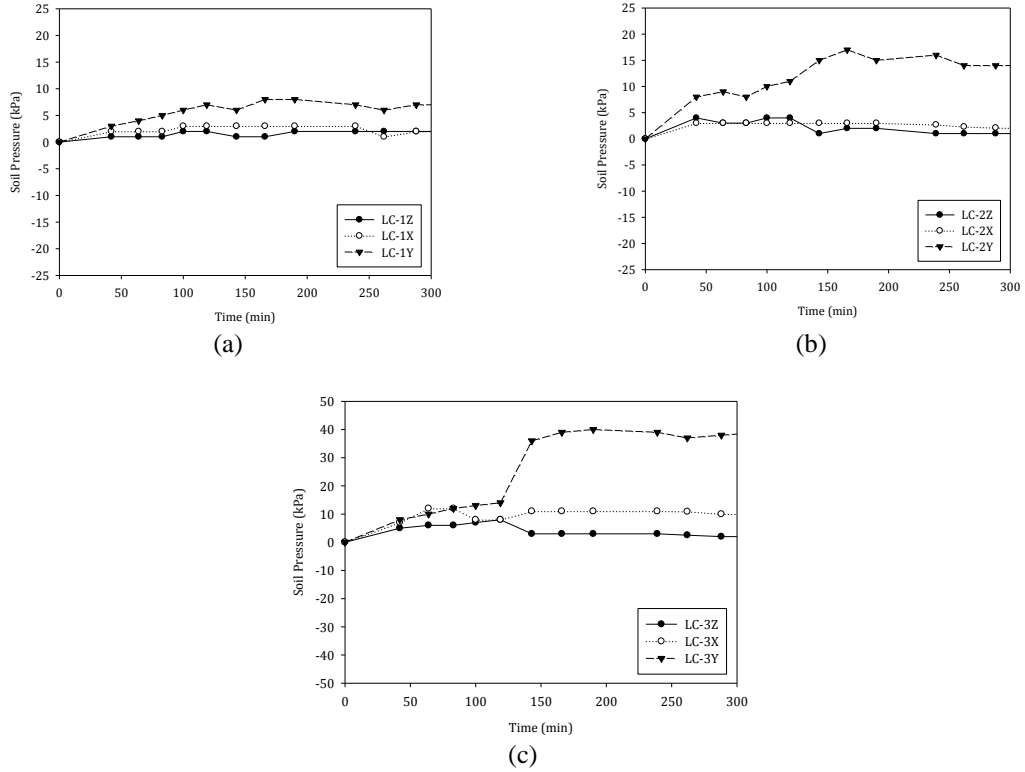
(a)



(b)



(c)

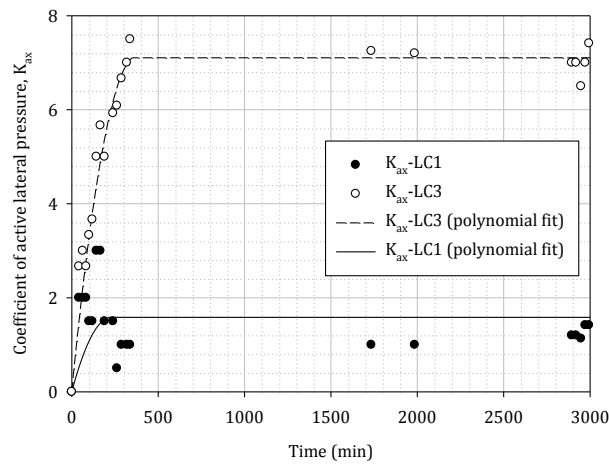Fig. 12 Variation of soil pressure in the tube



Fig. 13 Measured and fitted data points for the coefficient of lateral pressures at LC1 and LC3

In Fig. 13, it can be seen that the scatter plots for $K_{ax}$-LC1 are widely spread out compared to $K_{ax}$-LC3. This might be due to the unstable behavior of the unconsolidated fill material. As stated earlier, the nature of the confined fill material during the filling and dewatering stages cannot be considered as a normally consolidated soil due to the ongoing changes of the tubes shape and water content. Another factor that could have influence the results presented in Fig. 13 is the location of the pressure sensors. The pressure meters for LC3 are installed closer to the inlet of the tube and sensors for LC1 are installed farther. Since most of the coarser fills are deposited near the tube inlet, a more compact soil mass is form in the area, thus resulting to a much clustered data points in Fig. 13. On the other hand, finer particles are mostly deposited farther from the tube inlet containing high concentration of moisture content, thus exhibiting an unstable behavior as illustrated by widely spread scatter plots for LC1 in Fig. 13.

It can be seen from the graphical results presented in Fig. 12 that the confined fill materials at LC-1, LC-2 and LC-3 are subjected to non-isotropic states of stresses. To establish a three-dimensional stress relationship of the confined fill material, the total stress parameters $p$ and $q$ were determined and plotted. The total stress parameters $p$ and $q$ are used because it accounts for the mean stresses of the confined fill material. In this study, the $p$-$q$ graph is intended to illustrate the development of the stress path as the fill material accumulates inside the geotextile tube. The successive states of stresses experienced by the fill material confined in the geotextile tube during the progress of filling and dewatering at LC1, LC2 and LC3 are shown in Fig. 14. The total stress parameters $p$ and $q$ at the bottom of the tube were obtained using the following equations

$$p = \frac{1}{3}\left(\sigma_z + \sigma_x + \sigma_y\right) \tag{4}$$

$$q = \frac{1}{\sqrt{2}}\left[\left(\sigma_z - \sigma_x\right)^2 + \left(\sigma_x - \sigma_y\right)^2 + \left(\sigma_y - \sigma_x\right)^2\right]^{1/2} \tag{5}$$
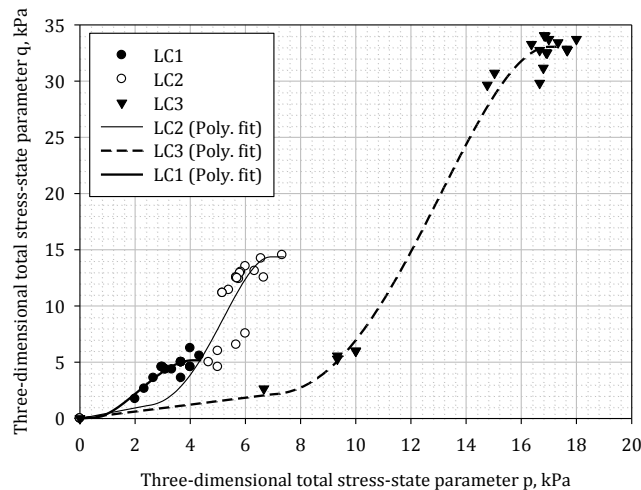


Fig. 14 Three-dimensional total-stress path

where $\sigma_z$ is the vertical pressure and $\sigma_x$ and $\sigma_y$ are the horizontal pressures measured by the load cells. The total stress paths at LC1, LC2 and LC3 show similar behavior. The magnitudes of the p and q parameters are higher in areas nearer to the inlet of the tube and lesser in areas farther from the inlet. The total stress parameter p increases in time with the total stress parameter $q$. As the soil reach into a stabilized state (soil fill is solidified), the total stress parameter $q$ normalizes. Similar trend for the increasing stress path can be seen from LC1, LC2 and LC3. The stress path increases as the loading increases due to the accumulation of fill materials inside the tube.

## 4. Conclusions

The large-scale apparatus introduced in this paper is useful for geotextile tube experiments particularly in the monitoring of the changes in its tube shape. The apparatus will be useful in future geotextile tube experiment. Based on the first experiments conducted the following conclusions are drawn:

- After the filling and dewatering processes, the properties of the soil fill in the tube shows an inhomogeneous characteristic throughout the geotextile tube's interior.
- Finer soil particles are found to be heavily deposited further from the inlet of the tube.
- A considerable change in the geotextile tubes shape (extensive decrease of tube height during the stabilization period) happens in areas where the soil deposits contains higher amount of moisture content and finer particles.
- The tangential strain of the geotextile tube varies around its circumference.
- Regardless of the magnitude, the strain readings showed that the deformation behavior of the geotextile tube is symmetrical for gauges located at the top and sides.
- The data readings are at minimal at the bottom of the tube. Presumably the stretching of geotextile at these locations are limited due to the confining effect between the soil fill and the foundation.
- Due to the variation of the strain distribution on the geotextile skin, the circumferential tensile force of the geotextile may as well be non-constant.
- A trend was shown that the total pressure on the longitudinal direction is significantly higher than the total pressures along the downward and transverse directions.
- During the dewatering stage, the tube height decreases and the tube width increases. This increases the density of the confined fill material and the tensile reaction of the tube. The compaction effect on top of the geotextile tube decreases as the tube height reduces. On the other hand, the confinement effect at the sides of the geotextile tube increases as the tensile reaction intensifies. As a result, the vertical pressure was decreased and the lateral pressures were increased, consequently increasing the coefficient of active earth pressure. This means that the contained fill material might fail and internally rearrange the soil particles due to the dewatering process. Therefore, in order to achieve external stability, the geotextile strength must be greater than that of the applied soil pressure.
- The coefficient of active pressure normalizes towards the end of the filling process of the geotextile tube.
- The stress path increases as the loading increases due to the accumulation of fill materials inside the tube.

## Acknowledgements

## References

Alvarez, I.E., Rubio, R. and Ricalde, H. (2007), "Beach restoration with geotextile tubes as submerged breakwaters in Yucatan, Mexico", *Geotext.Geomembranes*, **25**(4-5), 233-241.

Brink, N.R., Kim, H.J. and Znidarcic, D. (2013), "Consolidation modelling for geotextile tubes filled with fine-grained material", *Proceedings of the GhIGSGeoAfrica 2013 Conference*, Accra, Ghana, November.

Cantré, S. (2002), "Geotextile tubes – analytical design aspects", *Geotext.Geomembranes*, **20**(5), 305-319.

Cantré, S. and Saathoff, F. (2011), "Design method for geotextile tubes considering strain – formulation and verification by laboratory tests using photogrammetry", *Geotext.Geomembranes*, **29**(3), 201-210.

Das, B.M. (2010), "Principles of geotechnical engineering", (7th Ed.), Cengage Learning, Stamford, C.T., USA.

Fowler, J., Stephens, T., Santiago, M. and De Bruin, P. (2002a), "Amwaj Islands constructed with geotubes, bahrain", *Proceedings of the CEDA Conference*, Denver, USA.

Fowler, J., Ortiz, C., Ruiz, N. and Martinez, E. (2002b), "Use of geotubes in Columbia, South America", *Proceedings of the 7th International Conference on Geosynthetics*, Nice, France, Balkema.

Gibeaut, J.C., Hepner, T.L., Waldinger, R., Andrews, J.R., Smyth, R.C., Gutierrez, R., Jackson J.A. and Jackson, K.G. (2003), "Geotubes for temporary erosion control and storm surge protection along the Gulf of Mexico Shoreline of Texas", *Proceedings of the 13th Biennial Coastal Zone Conference*, Baltimore, MD, CD-ROM.

Kim, H.J., Lee, K.W., Jo, S.K., Park, T.W. and Jamin, J.C. (2014a), "The influence of filling port system to the accretion and pressure distribution of dredged soil fill in acrylic tubes", *Proceedings of the Advances in Civil, Environmental and Materials Research (ACEM14)*, Busan, Korea, CD-ROM.

Kim, H., Won, M. and Jamin, J. (2014b), "Finite-element analysis on the stability of geotextile tube–reinforced embankments under scouring", *Int. J. Geomech.*, 10.1061/(ASCE)GM. 1943-5622.0000420.

Kim, H.J., Won, M.S., Kim, Y.B., Choi, M.J. and Jamin, J.C. (2014c), "Experimental analysis on composite geotextile tubes hydraulically filled underwater condition", *Proceedings of the Advances in Civil, Environmental and Materials Research (ACEM14)*, Busan, Korea, CD-ROM.

Kim, H.J., Jamin, J.C. and Mission, J.L. (2013a), "Finite element analysis of ground modification techniques for improved stability of geotubes reinforced reclamation embankments subjected to scouring", *Proceedings of the Advances in Structural Engineering and Mechanics (ASEM13)*, Jeju, Korea.

Kim, H.J., Jamin, J.C., Won, M.S., Sung, H.J. and Lee, J.B (2013b), "A study on the behavior of dredged soil stratified in a transparent geobag", *Proceedings of the Advances in Structural Engineering and Mechanics (ASEM13)*, Jeju, Korea.

Koerner, G.R. and Koerner, R.M. (2006), "Geotextile tube assessment using a hanging bag test", *Geotext. Geomembranes*, **24**(2), 129-137.

Kriel, H.J. (2012), *Hydraulic stability of multi-layered sand-filled geotextile tube breakwaters under wave attack*, MSc Thesis, Stellenbosch University, South Africa.

Lawson, C.R. (2008), "Geotextile containment for hydraulic and environmental engineering", *Geosynth. Int.*, **15**(6), 384-427.

Leshchinsky, D., Leshchinsky, O., Ling, H.I. and Gilbert, P.A. (1996), "Geosynthetic tubes for confining pressurized slurry: some design aspects", *J. Geotech. Eng.*, **122**(8) 682-690.

Liu, G.S. and Silvester, R. (1977), "Sand sausages for beach defence work", *Proceedings of the 6th Australasian Hydraulics and Fluid Mechanics Conference*.

Moo-Young, H.K., Gaffney, D.A. and Mo, X. (2002), "Testing procedures to assess the viability of dewatering with geotextile tubes", *Geotext. Geomembranes*, **20**(5), 289-303.

Parab, S.R., Chodankar, D.S., Shirgaunkar, R.M., Fernandes, M., Parab, A.B., Aldonkar, S.S. and Savoikar, P.P. (2011), "Geotubes for beach erosion control in Goa", *Int. J. Earth Sci. Eng.*, **4**, 1013-1016.

Pilarczyk, K.W. (2008), "Alternatives for coastal protection", *J. Water Resources Environ. Eng.*, **23**, 181-188.

Plaut, R.H. and Klusman, C.R. (1999), "Two-dimensional analysis of stacked geosynthetic tubes on deformable foundations", *Thin Wall. Struct.*, **34**(3), 179-194.

Plaut, R.H. and Suherman, S. (1998), "Two-dimensional analysis of geosynthetic tubes", *Acta Mech.*, **129**(3-4), 207-218.

Recio, J. and Oumeraci, H. (2009), "Processes affecting the hydraulic stability of coastal revetments made of geotextile sand containers", *Coastal Eng.*, **56**(3), 260-284.

Restall, S.J., Jackson, L.A., Heerten, G. and Hornsey, W. P. (2002), "Case studies showing the growth and development of geotextile sand containers: an Australian perspective", *Geotext. Geomembranes*, **20**, 321-342.

Weggel, J.R., Dortch, J. and Gaffney, D. (2011), "Analysis of fluid discharge from a hanging bag", *Geotext. Geomembranes*, **29**(5), 65-73.